Limnol. Oceanogr., 47(3), 2002, 656–671

Spatial-temporal variability in surface layer deepening and lateral advection in an embayment of Lake Victoria, East Africa

Sally MacIntyre
Institute for Computational Earth System Science and Marine Science Institute, University of California, Santa Barbara, California 93106-6150

José R. Romero
Centre for Water Research, University of Western Australia, Crawley, WA 6009, Australia

George W. Kling
Department of Ecology and Evolutionary Biology, University of Michigan, Ann Arbor, Michigan 48109-1048

Abstract

Vertical and horizontal exchanges in Pilkington Bay, a shallow (9 m) embayment of Lake Victoria, were determined from a surface energy budget, time series measurements of temperature, and quasi synoptic transects of conductivity, temperature, and depth conducted over a 2-d period. The surface energy budget is the first from a tropical lake over a diurnal timescale. Strong stratification developed during morning and early afternoon (>40 cycles h^{-1}) but was eroded beginning in the afternoon by the combination of wind and heat loss. Surface heat losses contributed $>70\%$ of the energy for surface layer deepening 82% of the time from midafternoon until midmorning. Circulation times of the surface layer were <2 min as it deepened to 1.5 m in the afternoon and were <12 min at night even when mixing extended to the lake bottom. Spatial differences in the rates of heating and cooling and in the depth of wind mixing caused fronts to develop on spatial scales of kilometers within the bay. Convergence of these fronts led to downwelling of surface waters and upwelling of deep waters during the stratified period. Horizontal pressure gradients due to differential heating contributed to thermocline downwelling, lateral movement of deep, anoxic waters, and generation of high-frequency internal waves, all of which contribute to vertical and horizontal transports. Although wind and heat loss at one location generally determine the depth of the surface layer and thermocline, the depths of these key features may be strongly influenced by rates of heating and cooling elsewhere in a basin.

The temporal and spatial scales of advection and vertical mixing determine the flux paths of particles and solutes in aquatic ecosystems and, ultimately, lacustrine productivity. Time series measurements of surface meteorology, from which surface energy budgets can be calculated, and water column temperatures can be used as an indirect approach to determine these pathways. The data also can be used to determine internal wave dynamics, the energetics of mixing, and the role of intrusions and density driven flows in advection. With this information, the rates of circulation within the upper mixed layer and vertical and horizontal transports can be assessed.

The diurnal cycle of stratification and mixing is determined by the surface energy budget. Imberger (1985) provided the first quantitative description of the surface energy fluxes and their impacts on the upper part of a water column and the seasonal thermocline. He defined the surface layer as the region of the upper mixed layer directly affected by wind forcing and surface heating. It is actively mixing, whereas the waters below may not be. Additional studies of the short-term dynamics of the surface layer of temperate lakes include Ishikawa and Tanaka (1993), MacIntyre (1993, 1996, 1998), and Robarts et al. (1998). Oceanographic studies have also elaborated on the strong coupling between surface forcing and dynamics of the surface layer, subsurface layer, and thermocline (Brainerd and Gregg 1993*a*,*b;* Anis and Moum 1994, 1995). Together, these studies have documented the deepening of the surface layer at night from heat loss and wind forcing, the reestablishment of the diurnal thermocline during the day because of solar heating, and the daytime decay of turbulence within the subsurface layer between the diurnal thermocline and the seasonal thermocline.

In tropical lakes, the upper water column stratifies in the day but becomes nearly isothermal by daybreak (MacIntyre and Melack 1982, 1984, 1988, 1995; Melack 1982; Hare and Carter 1984; Powell et al. 1984). Whether the whole water column mixes depends on lake depth. Typically, wind forcing was low at night during these studies, which indicates the importance of heat loss to mixed-layer deepening. Di-

Acknowledgments

The Fisheries Research Institute in Uganda provided permission, encouragement, and help in many ways for this research. We thank Fred Bugenyi, Rose Mugidde, Moses Magumba, Patricia Ramlal, and the captain and crew of the R/V *Ibis* for their great support in the field and in the laboratory. Financial support was provided by National Science Foundation grants DEB95-53064 to G.W.K., DEB93-18085 to G.W.K. and S.M. and DEB93-17986, 97-26932, and OCE99-06924 to S.M. and by the Centre for Water Research, University of Western Australia, to J.R. We thank Lorenz Moosmann for his assistance with data analysis and graphics and John Melack, Bob Hecky, Dan Livingstone, Erika McPhee, and Bill Shaw for critically reading the manuscript. Comments from two anonymous reviewers were extremely helpful.

urnal studies at Lake Sonachi, Kenya, provided the first descriptions of the resistance of the surface layer to wind mixing during the day due to strong solar heating and the deepening of the surface layer at night due to surface cooling (MacIntyre and Melack 1982).

The structure of the upper mixed layer is not determined by surface forcing at only one site. Studies in small lakes and in the laboratory have demonstrated that horizontal density differences associated with spatial variations in the rate of heating, cooling, and the depth of wind mixing lead to horizontal overflows and to gravity currents at depth (Imberger and Parker 1985; Monismith et al. 1990; Coates and Ferris 1994; Sturman et al. 1996). Overflows can occur during wind forcing (Parker and Imberger 1986) and may lead to subtle temperature differences within the mixed layer that restrict the depth of surface overturns and prevent full circulation (MacIntyre 1998). Consequently, understanding upper mixed–layer dynamics requires consideration of processes occurring elsewhere in a lake.

Recent studies have also shown that a one-dimensional approach is not sufficient for understanding vertical transport through the thermocline. Turbulence at the boundaries of lakes can exceed that in the central portion by up to four orders of magnitude (Goudsmit et al. 1997; MacIntyre et al. 1999; J. Imberger unpubl. data). Intrusions from mixing at the boundary (Thorpe 1998) or other advective processes serve to redistribute the mixed fluid. Vertical exchanges can also occur from upwellings or downwellings induced as horizontal temperature gradients change sign because of more rapid heating and cooling in nearshore than offshore waters (Farrow and Patterson 1993).

Physical processes affect ecosystem functioning in a variety of ways. For instance, the energetics of the surface layer are crucial for gas fluxes (Crill et al. 1988), the light history of phytoplankton (MacIntyre 1993, 1998), and redistributing nutrients throughout the euphotic zone (MacIntyre and Melack 1995). Boundary mixing in a large lake has been shown to supply nutrients to a deep chlorophyll maximum (MacIntyre et al. 1999) and to reduce nutrient limitation at the base of the upper mixed layer (MacIntyre and Jellison in press). In a shallow, well-oxygenated basin of Lake Biwa, wave-induced sediment resuspension was more important for phosphorus supply than advection from an internal surge or nocturnal cooling (Robarts et al. 1998). James and Barko (1991) and Nepf and Oldham (1997), in shallow embayments, documented differential heating and cooling as the hydrodynamic processes that control the supply of nutrients and toxic substances upward to the surface layer or downward to the thermocline and deeper waters.

A wide variety of physical processes co-occur in lakes and interact in ways that presently cannot necessarily be predicted. Differential heating and cooling and wind mixing are particularly likely to occur in lakes with complex geometries but have not been examined on a basin scale. To develop an understanding of the flow paths that occur in a tropical lake with complex morphometry, we undertook a study of Pilkington Bay, a shallow, eutrophic embayment in northwestern Lake Victoria, East Africa. This 44 km^2 bay is similar to a moderately sized lake. It has a complex geometry, rather than a spherical one, and, hence, is more likely to be strongly influenced by differences in rates of heating, cooling, and depth of wind mixing than a lake with a simple shape. Lakes with complex geometry are ubiquitous. For instance, the Amazon basin, one of the largest lake districts in the world, is replete with lakes of complex geometries (Sippel et al. 1992). Hence, Pilkington Bay is illustrative of a large class of lakes worldwide. Because of its connection with other embayments and channels, an understanding of the exchange through these connections will have applications to other lakes with connections to either coastal waters, another lake, or a riverine system. In addition, Pilkington Bay's geometry is similar to that of bays found inshore throughout Lake Victoria. Thus, we anticipated that this study would likely lead to an understanding of the flows from inshore to offshore waters that have contributed to the eutrophication of Lake Victoria.

In the following, we describe the spatial and temporal variations in thermal structure of Pilkington Bay with time-series measurements of temperature at a central station, quasi synoptic north-south and east-west transects across the bay with conductivity-temperature-depth (CTD) profiling, and surface meteorology over two diel cycles. Data were collected during periods of strong heating, cooling, and wind forcing. We quantify the surface energy budget and use it to determine whether wind forcing or buoyancy forcing due to heat losses drives mixed-layer deepening and rates of mixing in the upper water column. We use CTD transects to illustrate the frontal structures that develop on kilometer scales because of different rates of heating and cooling and depths of wind mixing. We assess the resulting vertical transports and horizontal advection and provide evidence for intrusions from outside the Bay. We show that horizontal inflows can influence the depth of the surface layer and cause thermocline tilting and subsequent generation of high frequency waves. We calculate the likelihood of localized mixing at the boundaries of the bay due to these waves. With these various measurements, we illustrate the processes that regulate transport of particles, solutes, and gases and the resulting flow paths in a moderately sized water body.

Study site—Lake Victoria (Fig. 1), the second largest freshwater lake in the world in terms of surface area (~68,800 km^2), has changed substantially over the past 40 yr because of the effects of cultural eutrophication (Bootsma and Hecky 1993; Hecky 1993) and introduced predatory fish (Kaufman 1992, 1993). Pilkington Bay (00°17′N, 33°20′E) lies between the two arms of Buvuma Island near the outflow of the Nile River from Lake Victoria. The bay has a surface area of ~40 km^2 and an average depth of ~4.5 m. Lingira Island splits the bay opening into two channels; the deeper (>10 m) northern channel connects to Buvuma Channel and the shallower (8 m) eastern channel connects to Hannington Bay. A 16-m ''hole'' at the western boundary of the northern channel opening is the deepest point in the bay. The bay is clover-leafed in shape, with three lobes. The western and southern lobes have greater areas than the eastern lobe. The central bay varies in depth from 6 to 10 m. Papyrus fringes much of the shoreline along the southern and western lobes.

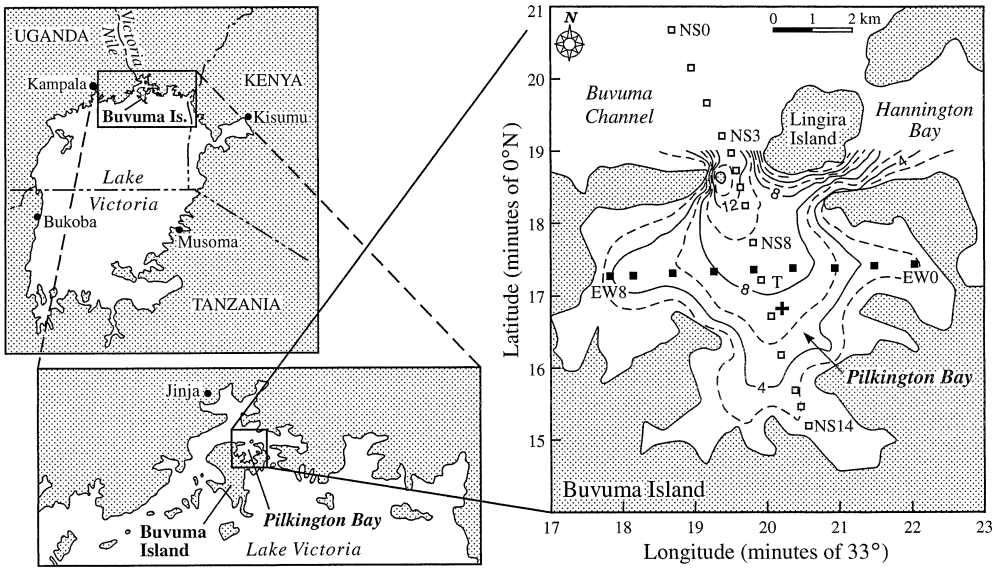

Fig. 1. Locator map for Lake Victoria and Buvuma Island, detail map of northern end of Lake Victoria showing Pilkington Bay in Buvuma Island, and bathymetry of Pilkington Bay with contours at 2-m intervals. North-south and east-west CTD transects with Sta. EW0, EW8, NS14, NS8, NS3, and NS0 labeled. The cross (+) in the middle of the bay is the location of the limnological sampling and meteorological stations on the R/V *Ibis.* **T** is the location of the thermistor chain near the intersection of the two transects. Lingira Island bisects the bay opening to the north into northern and southern entrances connecting to Buvuma Channel and Hannington Bay, respectively.

Methods

Bathymetry—The bathymetry of Pilkington Bay was derived from depth soundings within the bay, the bay entrance, and near-entrance regions of Buvuma channel on several occasions from 1994 to 1996. Accuracy is ±0.3 m.

Transects—The Pilkington Bay field study was conducted over 51 h from 1115 h on 24 April to 1450 h on 26 April 1996 (Table 1). The thermistor chain and meteorological instrumentation were moored near the center of the bay (Fig. 1). Eleven north-south and eight east-west transects were made during the study (Table 1). The stations along the north-south transect were ~1 km apart in the bay and channel but had 0.5 km spacing across the bay entrance (Sta. NS3–NS7) and the southern portion of the transect (Sta. NS12–NS14). The stations along the east-west transect were spaced 1 km apart except at the western margin, where EW8 was 0.5 km from EW7. At each station a CTD profile was taken, and during daylight a Secchi depth was measured. The east-west transect had a total of 9 stations, and the north-south transect had 15.

Vertical profiles of pressure, temperature (°C), and conductivity (μS cm^{-1}) were made with a CTD profiler (Sea-Bird SBE19, Seacat) at each transect station. The CTD samples at 2 Hz and was lowered at a descent rate of ~50 cm s^{-1}. CTD sampling was quasi synoptic, because the north-south and east-west transects were performed in ~1 hr and ~45 min, respectively. Density was calculated by use of the international equation of state (IES) for seawater (Millero and Poisson 1981). Results were verified against an approach that used partial molal volumes (Kling et al. 1989) and against the method of Chen and Millero (1977), which was designed for freshwater. Differences between approaches were small; $\sim 8 \times 10^{-6}$ g cm^{-3} between IES and Chen and Millero and $\sim 5 \times 10^{-5}$ g cm^{-3} between IES and the partial molal volume approach. These results indicate that the contribution of dissolved salts to density is minor. The stability of the water column is calculated as the buoyancy frequency, $N = (g/\rho\, d\rho/dz)^{1/2}$ where g is gravity and ρ is density.

Time-series temperature measurements—Sixteen self-contained temperature loggers (WaDaR, Model TL; TSKA) were deployed at the intersection of the two transects (Fig. 1B). The surface thermistors were deployed at 0.1 and 0.5 m and, thereafter, at 0.5-m intervals to a depth of 5.5 m. The depth at the station was ~8 m, so the bottom two thermistors were deployed at 6.5 and 7.5 m. The thermistors are accurate to 0.01°C, have a resolution of 0.0014°C, and have a response time (67% of a step change in temperature) of ~3 min. The sensors were sampled every 30 s. Isotherm depths were calculated from linear interpolation between the depths of the WaDaRs. All WaDaR sampling times were synchronized. Spectra of isotherm displacements were computed by use of a Hanning window with 75% overlap of windows and linear detrending. Differences in location and magnitude of spectral peaks were subtle based on comparisons between detrending using the mean or linearization; 80% confidence intervals were computed, and a sliding window size was used to increase resolution at high frequencies.

Current measurements—Drogue measurements were made on two occasions near the thermistor chain. The drogues were constructed from canvas fastened to a PVC

Table 1. Sampling times, locations, and weather conditions.

Time (h)	Station(s)	Type
24 Apr 1996		
1115	T	Thermistor chain recording
1125–1234	North → south	NS transect hot and calm
1300–1342	East → west	EW transect 1, hot and calm
1540–1640	North → south	NS transect 2, SE wind in N, calm S of midbay
1700–1735	East → west	EW transect 2, hot and calm
1935–2035	North → south	NS transect 3, waves 20 cm in channel, 10 cm near bay entrance, calm in shallows
2050–2125	East → west	EW transect 3, calm
2250–2320		Thunderstorm, high winds
25 Apr 1996		
0055–0151	North → south	NS transect 4, calm and light drizzle
0210–0247	East → west	EW transect 4, calm and light drizzle
0630–0700		High winds
0740–0845	North → south	NS transect 5, waves 15–20 cm in channel to calm in shallows
0907–0942	East → west	EW transect 5, calm
1138–1243	North → south	NS transect 6, calm in channel to 5-cm waves in shallows
1300–1337	East → west	EW transect 6, 10-cm waves
1550–1654	North → south	NS transect 7, 5–10 cm waves, calmer in shallows
	B	Drogue measurements, no EW transect 7
1937–2030	North → south	NS transect 8, 15-cm swell in channel, calm in bay
2046–2117	East → west	EW transect 8, calm
26 Apr 1996		
0007–0057	North → south	NS transect 9, 15-cm swell in channel, calm in bay
0113–0144	East → west	EW transect 9, calm
0300–0430		Biggest wind storm
0937–1035	North → south	NS transect 10, 20-cm swell in channel, 5–10-cm waves in bay, calm in shallows
1100–1135	B	Drogue measurements
1353–1450	South → north	NS transect 11, 5-cm waves in shallows, 10–20-cm in channel

pipe frame. The drogues had four panels radiating perpendicularly from the center axis. Two drogue sizes were deployed: 0.3 × 0.45 and 0.6 × 0.75 m, for near-surface and middepth current measurements, respectively. A buoy was deployed at the starting location, and then the drogues were released. After 10–20 min, the distance from the buoy to the drogue was measured with a marked line and the current direction estimated with a compass. The current velocity was estimated as the travel distance divided by the time of deployment.

Surface meteorology—The meteorological station was mounted on the R/V *Ibis* at a height of ~5.0–5.5 m above the water surface. The R/V *Ibis* was moored ~1 km south of the intersection of the two transects (Fig. 1). Relative humidity, wind speed, shortwave radiation, air temperature, and rain were measured, but unfortunately the wind-direction vane did not function. Data were collected every 5 s and averaged over 5-min periods. Profiles of photosynthetically active radiation (PAR) at 0.5-m intervals were measured at the R/V *Ibis* with a Li-Cor meter and a 2π sensor. PAR extinction coefficients η were calculated with Beer's Law. The regression between Secchi depths and PAR extinction coefficients from Lake Victoria during 1994–1996 yielded the relation $\eta = 1.13\, z_{\text{secchi}}^{-0.82}$, $r^2 = 0.82$, $n = 43$, where η has units m^{-1} and secchi depth is in meters.

Surface energy fluxes—Estimates of the momentum, sensible heat, and latent heat fluxes were made with the bulk aerodynamic formulas, $\tau = \rho_A C_D U_Z^2$, $H = \rho_A C_{\text{Pa}} C_H U_Z (T_S - T_Z)$, and $E = \rho_A L_V C_E U_Z (q_S - q_Z)$, where τ is the shear stress of the air at the surface interface (N m^{-2}), ρ_A is the density of the air at the air-water interface (kg m^{-3}), C_D is the drag coefficient, U_Z is the wind speed at height z above the water surface (m s^{-1}), H is the sensible heat transfer (W m^{-2}), C_{Pa} and C_{Pw} are the specific heat of air and water (J kg^{-1} °C^{-1}), C_H is sensible heat transfer coefficient, T_S is the water surface temperature (°C), T_Z is the air temperature (°C) at height z, E is the latent heat transfer (W m^{-2}), L_V is the latent heat of vaporization (J kg^{-1}), C_E is the latent heat transfer coefficient, q_S is the specific humidity at saturation pressure at T_S, and q_Z is the specific humidity of the air at z. U_Z was measured ~5.5 m above the water surface; T and relative humidity (RH, %) were measured ~5 m above the water surface.

At diel time scales, the thermal inertia of the water is too

great to use constant values of the mass-transfer coefficients (C_D, C_H, and C_E), and atmospheric stability must be included. Following the method of Monin and Obukhov (1954), we parameterized the nondimensional gradients of wind, potential energy, and specific humidity in terms of the stability parameter zL^{-1}, where

$$L = \frac{-\rho_A u_*^3 T_V}{kg\left(\frac{H}{C_{\mathrm{Pa}}} + 0.61\frac{T_z E}{L_V}\right)}$$

L is the estimate of the Monin and Obukhov length scale (m), g is the gravitational acceleration (m s^{-2}), T_V is the virtual air temperature ($=T_Z[1 + 0.61q_Z]$, °K), k is the von Karman constant (= 0.4), and air shear velocity $u_* = (\tau/\rho_a)^{0.5} = (C_D U_Z^2)^{0.5}$.

Neutral values of the transfer coefficients at 10 m are C_{DN} (1.0×10^{-3}), C_{HN} (1.35×10^{-3}), and C_{EN} (1.35×10^{-3}) (Hicks 1972, 1975; Pond et al. 1974; Rayner 1981), which need to be adjusted for measurement height. We adjusted C_{DN} to 5.5 m following the method of Amorocho and DeVries (1980). Neutral transfer coefficients corrected for measurement height were 1.1×10^{-3} for C_{DN} and 1.54×10^{-3} for C_{EN} and C_{HN}.

The iterative approach suggested by Hicks (1975) was used to estimate transfer coefficients corrected for atmospheric stability. Initially, neutral values of the transfer coefficients (C_{DN}, C_{EN}, and C_{HN}) were used to calculate neutral fluxes. From these results, transfer coefficients were obtained from the similarity functions of Paulson (1970) for both the unstable ($zL^{-1} < 0$) and stable cases ($zL^{-1} > 0$). Four iterations were the maximum required for L to converge within 0.001% of the previous L. A cutoff of $|zL^{-1}| < 15$ was imposed during the computation of the stability parameter; hence, the smallest values of L were ~0.4 m. This arbitrary cutoff follows bounds set by Imberger and Patterson (1990).

Incoming and emitted longwave radiation were calculated separately prior to determining net longwave radiation. Formulations of net longwave radiation are based on either air or surface water temperature and cloud cover (Henderson-Sellers 1986). Emitted longwave radiation was calculated as $LW_{\mathrm{Out}} = \varepsilon_w \sigma T_s^4$, where ε_w is the emissivity of water (0.97 ± 0.005) (Anderson 1954), σ is the Stefan-Boltzman constant ($=5.67 \times 10^{-8}$ W °K^{-4} m^{-2}), and T_s is the surface water temperature (°K). Incoming longwave radiation was calculated under the assumption that the emissivity of air, ε_a, is given by a formula for cloudless conditions and a simple multiplicative factor of $(1 + k_1 C^2)$ accounts for the fraction of cloud cover, C, where k_1 is a constant equal to 0.17. Hence, incoming longwave radiation was calculated as $LW_{\mathrm{In}} = \varepsilon_a \sigma T_a^4 (1 + k_1 C^2)$, where the emissivity of air, ε_a, was calculated as $\varepsilon_a = 0.642(e_a/T_a)^{1/7}$, where e_a is the vapor pressure of the air (Pa) and T_a is the air temperature (°K), a formulation based on theoretical considerations (Brutsaert 1982). Cloud cover observations were made throughout the study and served as inputs to calculate longwave radiation. The net surface heat flux (S, W m^{-2}), omitting short wave radiation, is thus $S = LW_{\mathrm{in}} - LW_{\mathrm{out}} + E + H$.

Surface heat and buoyancy fluxes—The diurnal mixed-layer dynamics were evaluated by use of the methods of Imberger (1985). To determine whether the surface layer was gaining or losing heat, we calculated the effective surface heat flux, H^* (W m^{-2}), defined as

$$H^* = S + q(0) + q(h) - \frac{2}{h}\int_h^0 q(z)\, dz$$

where $S = \rho_0 C_{\mathrm{Pw}} \langle w'T'(0) \rangle$ is the surface heat flux, h is the depth of the surface layer (m), $q(0)$ is the shortwave radiation at the surface (W m^{-2}), and $q(h)$ is the shortwave radiation at the bottom of the surface layer (W m^{-2}) (Kim 1976). The surface layer depth was defined as the first depth where the temperature difference was >0.02°C relative to the surface temperature located at 0.1 m. The penetration of radiation into the water column was parameterized with Beer's Law by use of seven-wavelength bands (Jellison and Melack 1993). Angle of refraction was included in the calculation.

The buoyancy flux, B (m^2 s^{-3}), is defined as $B = g\alpha H^*/(C_{\mathrm{Pw}}\rho_0)$, where the thermal expansion coefficient, α, in the range 20°C–30°C can be estimated from $\alpha = 1.6 \times 10^{-5} + 9.6 \times 10^{-6}\, T$, where T is in °C. The penetrative convection velocity, w_*, was calculated as $w_* = (Bh)^{1/3}$ (Deardoff 1970). The surface water shear velocity was calculated as $u_{*w} = (\tau/\rho_0)^{0.5}$, where ρ_0 is the density of water. The relation is based on the equality of shear on both sides of the air-water interface. The mechanical energy introduced at the water surface was derived from the work done by pressure fluctuations, the shear production in the wind surface layer, and from surface cooling. Kim (1976) showed that the energy flux F_q derived from these sources can be parameterized as $F_q = 0.5(w_*^3 + C_N^3 u_{*w}^3)$, where $C_N = 1.33$ (Rayner 1981).

Results

Meteorological forcing at the central bay station—Marked diel patterns were observed in air temperature, relative humidity, and shortwave radiation at the central bay station (Fig. 2). Except for a brief period in the early afternoon at the beginning of the study, air temperatures were generally >2°C cooler than the surface waters at the midbay station and throughout the bay. Consequently, the boundary layer above the air-water interface was unstable. Maximum air temperatures were several degrees warmer on 24 April than the other two days, and minimum air temperatures were cooler on 26 April than on 24 or 25 April. Relative humidity was least in late morning and during the afternoon and was >75% at other times. Shortwave radiation (280–2800 nm) peaked between 1000 and 1200 W m^{-2}. Fluctuations in irradiance indicated cloud cover, with greater coverage in the morning. A large fraction of the sky was covered with clouds from 0000–1200 h on 25 April and 0200–1300 h on 26 April (not shown).

On both 24 and 25 April, a land breeze generated moderate winds in the afternoon that persisted for at least 4 h (Fig. 2D). Relatively calm conditions with wind speeds <4 m s^{-1} bracketed both of these diurnal wind events. Winds were >8 m s^{-1} for up to 1.5 h on 24 April, beginning at

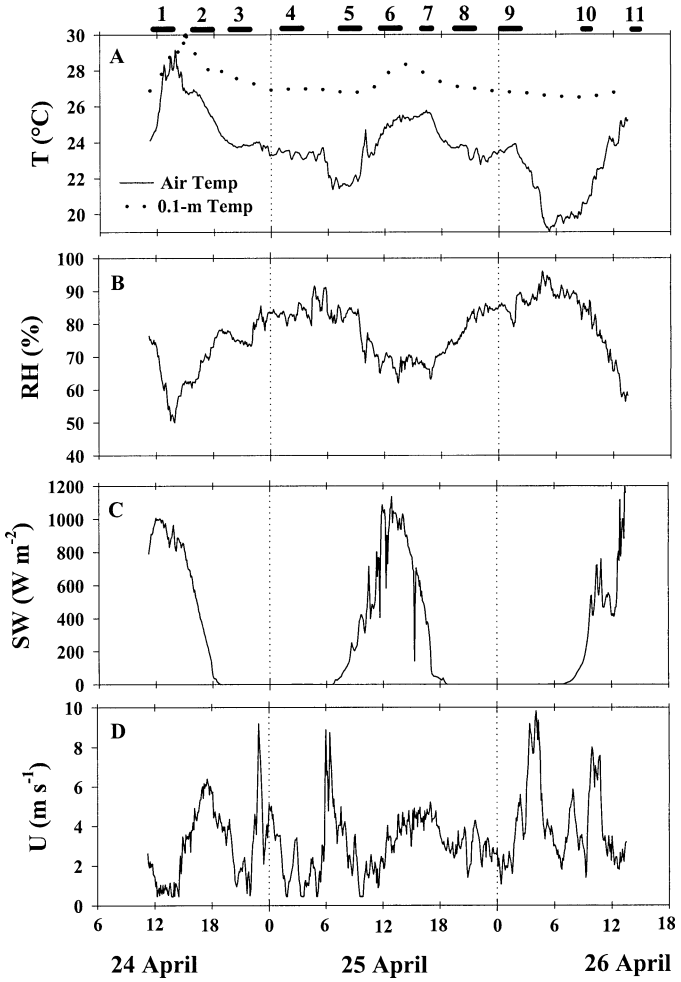

Fig. 2. (A) Air temperature and water surface temperature at 0.1 m at the thermistor chain, (B) relative humidity, (C) shortwave (280–2800 nm) solar radiation, and (D) 5-min averaged wind speed during the field study. Numbers and bars at top of temperature panel correspond to north-south CTD transects conducted over the course of the diel study (see Table 1). All meteorological measurements were recorded 5.0–5.5 m above the lake surface.

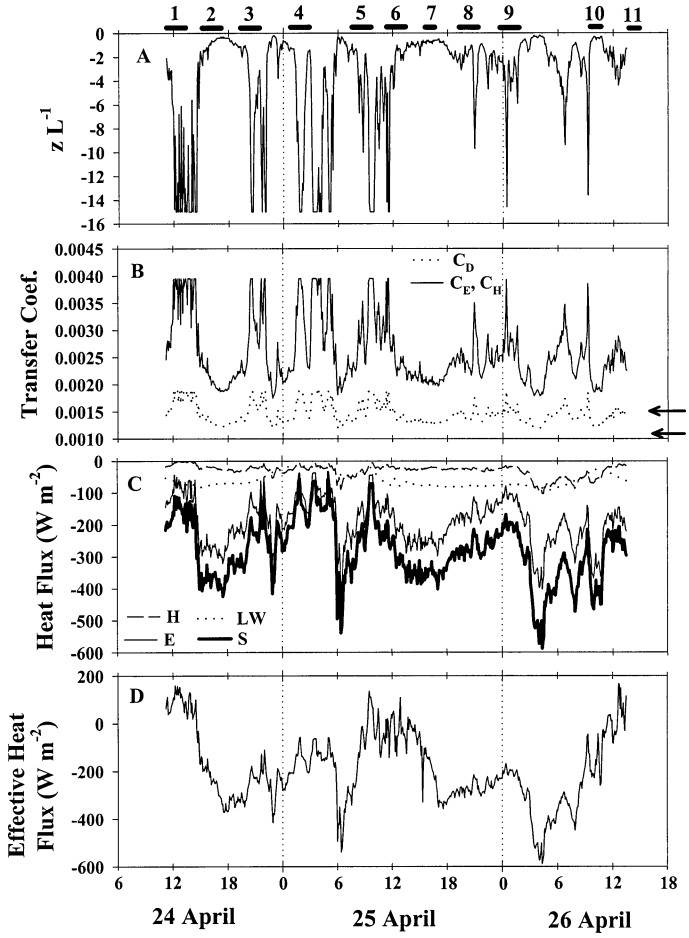

Fig. 3. (A) Air column stability parameter, zL^{-1}. (B) Mass (C_E), heat (C_H), and momentum (C_D) transfer coefficients corrected for atmospheric stability. Arrows indicate neutral transfer coefficients for mass and heat (upper) and momentum (lower). C_E and C_H are equal. (C) Surface heat flux components of sensible heat (H), latent heat (E), and net longwave radiation (LW) computed over 5-min intervals. S indicates the sum of H, E, and LW. (D) Effective heat flux into the surface layer.

2300 h, on 25 April just before sunrise, and on 26 April at 0300 and 1000 h.

The boundary layer above the air-water interface was unstable ($zL^{-1} < 0$) during the entire study, so that estimates of the transfer coefficients of heat, mass, and momentum were greater than neutral values (Fig. 3A,B). During low wind conditions, the stability parameter (zL^{-1}) was low (about -15), and the transfer coefficients were large because buoyancy effects dominated. Conversely, as the stability parameter approached zero during high winds, transfer coefficients approached their neutral values.

Surface heat losses were dominated by latent heat transfer (Fig. 3C). The sensible heat loss and net longwave radiation ranged from 0 to -100 W m^{-2}. The evaporative heat flux ranged from -50 to -100 W m^{-2} during low winds (<1–2 m s^{-1}) and was about -350 W m^{-2} for winds >8 m s^{-1}. Surface heat fluxes ranged from -100 to -200 W m^{-2} during low winds during the day, were -350 to -400 W m^{-2} during afternoon winds, and were up to -600 W m^{-2} during high winds. The effective heat flux into the surface layer had maximal values of 175 W m^{-2} and was often negative during the day (Fig. 3D). These low values relative to shortwave irradiance (Fig. 2C) indicate that little heat was being stored in the shallow surface layer in the day. Instead, considerable heating occurred below the surface layer.

The surface layer was shallower during the day and deepened at night (Fig. 4A). The most rapid deepening occurred subsequent to the strong wind forcing at 2300 h on 24 April, 0600 h on 25 April, and 0400 h on 26 April. The thermocline upwelled at 0300 h on 25 April.

The surface friction velocity, u_{*w}, proportional to the surface shear stress, indicates the magnitude of the turbulent velocity scale in the water due to wind forcing. During afternoon winds, u_{*w} was $\sim$0.007 m s^{-1}; during the strong wind forcing at night u_{*w} was 0.01 ms^{-1}. The convective velocity scale due to surface heat loss is w_* (Fig. 4B). This term was near 0 at midday, when solar heating was greatest,

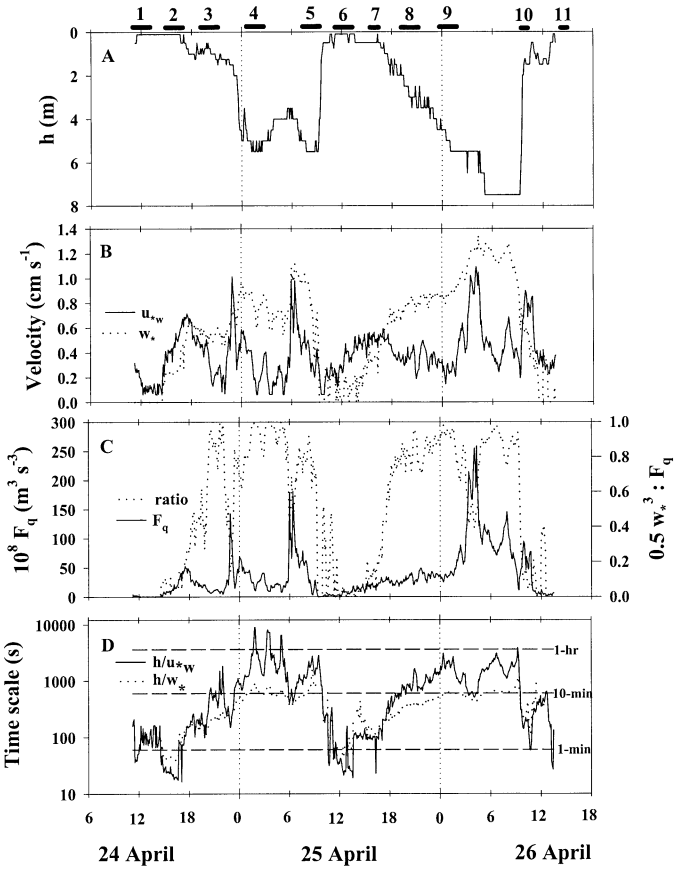

Fig. 4. (A) Depth of the surface layer (h), (B) convective (w_*) and shear (u_{*w}) velocity scales, (C) mechanical energy flux (F_q) and the fraction of F_q derived from the buoyancy flux ($0.5\ w_*^3$: F_q), and (D) convective (h/w_*) and shear (h/u_*) timescales of vertical mixing within the surface layer.

and began to increase by midafternoon as evaporation increased and shortwave radiation decreased. w_* was maximal during periods of high wind forcing at night and was $\geq u_{*w}$ from late afternoon until early morning.

The total turbulent energy flux into the surface layer, F_q, incorporates the energy due to the wind as well as the contribution from the surface heat flux (Fig. 4C). This term has its maximum values during periods with strong wind forcing when shortwave energy is low. Except during periods with high inputs of short wave energy or periods with high winds, buoyancy flux dominates the surface energy fluxes (Fig. 4C).

Time scales to mix the surface layer were most rapid during the day, when it was shallow (Fig. 4D). However, at night, the time scale for penetrative convection was nearly always <10 min, whereas that for wind stirring was generally longer and was sometimes >1 h.

Temperature time series at the central bay station—The diurnal cycle of heating and cooling and the effects of wind forcing on stratification are illustrated in Figs. 5–7. Strong diurnal heating, with surface temperatures reaching 30°C (Fig. 5), occurred on 24 April. The buoyancy frequency, which indicates the strength of stratification, was 49 cycles per hour (cph) in the upper half meter. This value is well in

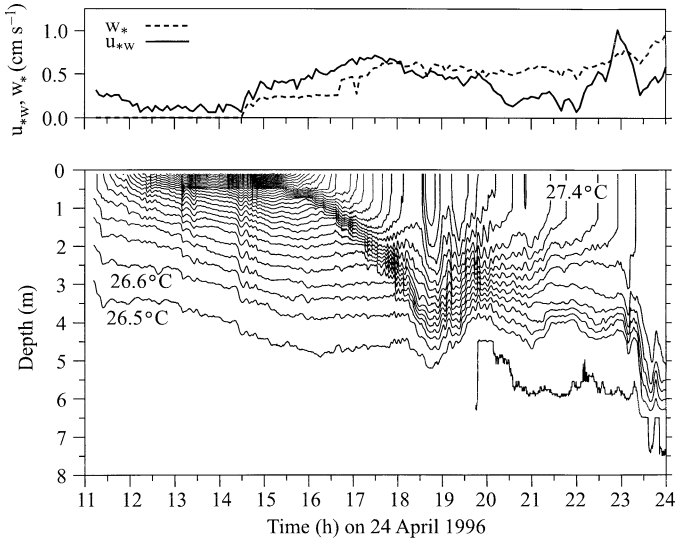

Fig. 5. u_{*w} and w_* (upper panel) showing increase in w_* as winds increase in afternoon and isotherms (lower panel) showing that stratification was initially to the surface and formation of a surface layer and diurnal thermocline as u_{*w} and w_* increased; 1100 to 2400 h on 24 April 1996. For temperatures >28°C, isotherms every 0.5°C; for lower temperatures isotherms every 0.1°C.

excess of 20 cph, a value indicative of strongly stratified oceanic waters, and is comparable to values observed in the seasonal pycnocline in dimictic lakes. After afternoon winds began and u_{*w} and w_* increased, the uppermost part of the water column began to lose heat and a diurnal thermocline formed with N decreasing to 25 cph. The thermocline downwelled until 1830 h and then upwelled, with the upwelling independent of surface forcing. During the upwelling, cool waters (26.4°C) flowed into the sampling region.

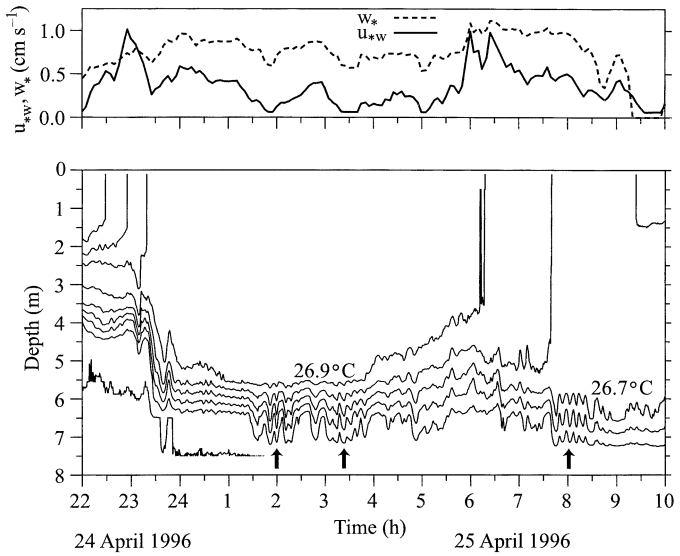

Fig. 6. As for Fig. 5 but for 2200 h on 24 April–1000 h on 25 April. The thermocline downwelled after strong wind forcing but remained downwelled and compressed when winds dropped. High-frequency waves (↑) occurred with decreases in u_*.

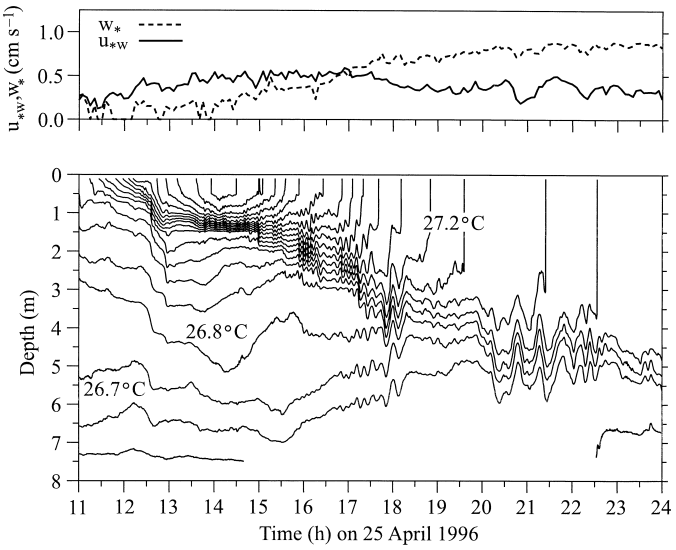

Fig. 7. As for Fig. 5 but for 1100–2400 h 25 April. Upwelling began at 1800 h independently of wind forcing, and high-frequency waves were generated after the downwelling at 1930 h.

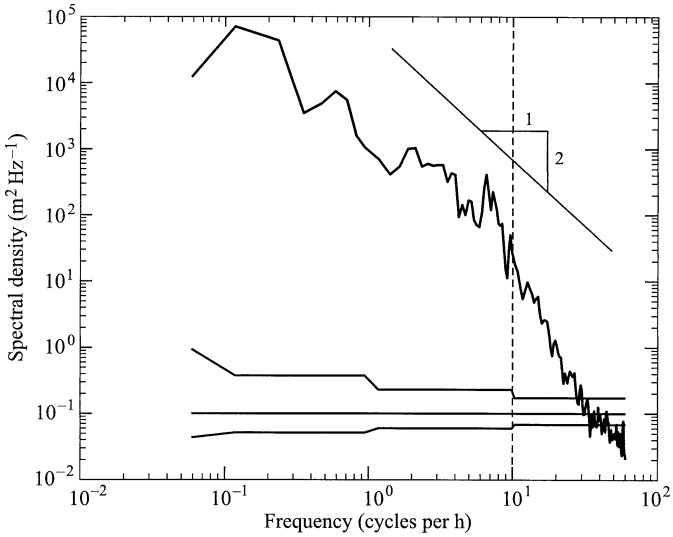

Fig. 8. Power spectrum of 26.6°C isotherm for period 2336 h on 24 April–0442 h on 26 April. The line in the upper right has a slope of −2, as is typical for oceanic waters and large lakes; 80% confidence intervals are indicated by stepped lines at the bottom of the figure. The length of Hanning windows decreased as frequency increases (2048, 1024, 512, and 256) to improve confidence. The dotted vertical line indicates buoyancy frequency at the depth of the isotherm.

Wind forcing reached 8 m s^{-1} twice during the period illustrated in Fig. 6, and u_{*w} reached 0.01 ms^{-1}. The thermocline downwelled after the initial forcing event but remained compressed despite low u_{*w}. High-frequency wave packets occurred in the thermocline coincidentally with lowest u_{*w} (Fig. 6, first two arrows). The thermocline gradually upwelled from 0400 to 0600 h, but wind forcing at 0630 h caused another slight downwelling. High-frequency waves were generated during relaxation from the second wind event (Fig. 6, third arrow). Maximum buoyancy frequencies in the thermocline during the night ranged from 11 to 17 cph.

Surface temperatures only reached 28.4°C on 25 April (Fig. 7). The morning was cloudy and windy, and development of thermal stratification was delayed until w_* dropped to 0 at 0920 h (Fig. 6). The stratification in the upper water column was weaker than during the previous day, because winds and intermittent cloud cover led to occasional heat losses from the upper water column during the morning heating period (Fig. 3C, 3D, 4B). The surface layer and diurnal thermocline began to form at 1230 h as u_{*w} reached 0.5 cm s^{-1}. The diurnal thermocline had a maximum buoyancy frequency of 46 cph at 1430 h. It progressively deepened during the afternoon, and maximal values of N decreased to 11 cph. Small-amplitude, high-frequency waves occurred frequently, likely because of gusts of wind. Movements of the 26.8°C and 26.7°C isotherms were out of phase from late morning until 1700 h. As will be discussed later, the separations are likely due to inflows from intrusions. Independently of wind speed, the thermocline upwelled at 1800 h and downwelled at 2000 h. After downwelling, a packet of waves was spawned with 1-m amplitude and periods <1 h. The thermocline continued to deepen after midnight, and by 0500 h the water column was isothermal (not shown).

Thermocline upwelling and downwelling was associated with inflows of cool water at depth. Cold inflows occurred at 1800 h on April 24 as the thermocline upwelled (Fig. 5), a warm inflow occurred at 1000 h on 25 April as the thermocline upwelled (not shown), and a cold inflow occurred at 2230 h on April 25 as the thermocline downwelled (Fig. 7).

Phase speeds of the first two vertical wave modes were calculated following the method of Monismith (1985, 1986, 1987), by use of profiles of buoyancy frequency over the diurnal cycle as input (not shown). Seiche periods were calculated as two times the length of the basin divided by phase speed. Because the shortest period of these calculated internal wave modes is ~1.5 d, wind forcing and nocturnal cooling would have disrupted basin scale modes before a cycle was completed. Consequently, the thermocline will not fully up or downwell because of wind forcing. Only higher harmonics of these waves and progressive waves are possible.

The power spectrum had a slope of −2 (Fig. 8) as has been observed in the ocean and other lakes (Saggio and Imberger 1998). Waves generated after the thermocline upwelled on 24 April had frequencies ranging from 0.36 to 0.9 cph (Fig. 5, 26.5°C and 26.6°C isotherms). Waves with frequencies between 0.3 and 12 cph were generated in the thermocline after midnight on 25 April (Fig. 6), and waves with frequencies between 1.5 and 3 cph were observed subsequent to thermocline downwelling (Fig. 7). Waves with a frequency between 2.2 and 9 cph were ubiquitous and appeared immediately after gusts of wind. Although there were no significant peaks in the spectrum, the data show the importance of changes in wind forcing and, as to be discussed later, the movement of water masses, for generating waves at moderate to high frequencies in the embayment.

Secchi depths—Large differences in Secchi depth occur within Pilkington Bay (Fig. 9). The waters were most turbid

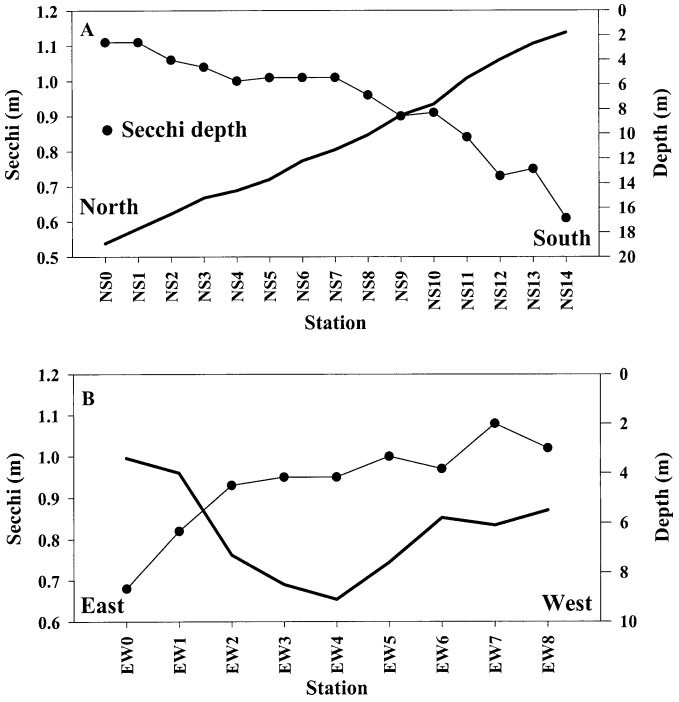

Fig. 9. Secchi depths increase (A) from south to north and (B) from east to west. Thick lines indicate depth of bottom.

at the southern end of the bay where the Secchi depth was 0.6 m. From NS7 into Buvuma Channel, the Secchi depths were between 1 and 1.1 m. In consequence, greater heating is expected in the most inshore southern portion of the bay than elsewhere, with rates of heating decreasing to the north. Similarly, a gradient in Secchi depths was measured along the east-west transect; Secchi depths increased from 0.7 m in the east to 1 m in the west. Hence, rates of heating in the very surface waters would be expected to be higher in the east.

Temperature transects—Upwelling, downwelling, and thermal fronts on horizontal scales of kilometers were documented by our CTD profiling (Figs. 10, 11). The most pronounced features on the north-south transect on 24 April included the downwelling of warm water at the mouth of the constriction between Pilkington Bay and Buvuma Channel (Fig. 10, transect 2), upwelling within Pilkington Bay just south of the upwelling (Fig. 10, transects 3 and 4), the development of pools of warm water on both sides of the upwelling, and the persistence of these warmer regions even during nocturnal cooling (Fig. 10, transects 3–5). Cool water (26.4°C) had moved to the thermistor station by transect 3. On 25 April, the entire water column was stratified in the late morning transect, a diurnal thermocline formed by mid-afternoon whose depth varied spatially. Below the diurnal thermocline, the 26.7°C isotherm rose and the 26.6°C isotherm was depressed between transects 7 and 8. These changes indicate an inflow of water with intermediate temperatures. By early evening, the thermocline was deeper, and, again, there were three pools of warmer water. The depth of strongest temperature gradient varied spatially. By early morning of 26 April, temperature stratification had weakened but the horizontal gradients in temperature had persisted throughout the night.

Occasionally, pockets of colder water would occur midbay near the bottom. Examples include the 26.5°C water at Sta. 9 and 10 on transect 3, the increased volume of cool water at Sta. 10 on transect 8, and the water 26.5°C and colder at Sta. 10 on transect 9 and at Sta. 11 on transect 10. Water cooler than 26.4°C was generally anoxic.

The dynamics of the east-west transect are similar, with stratification to the surface until early afternoon, the formation of a diurnal thermocline evident by late afternoon, and spatial variation in surface temperatures (Fig. 11). Surface temperatures were warmest to the east, and the depth of warmer water was greater there. On the initial transects on 24 April, the coldest bottom water was found on the east side of the basin. Cool water was found progressively farther west from the afternoon of 24 April until midmorning 25 April. This westward movement occurred coincidentally with thermocline deepening in the east.

Intrusions of warmer or colder water were noted on several transects. A cold water intrusion was found at 5 m on transect 3, and warm water intrusions occurred between 1 and 4 m at EW5 on transect 8, between 1 and 4 m between EW3 and EW4 on transect 9, and between 3 and 4 m depth between EW1 and EW2 on transect 9.

Discussion

Diel cycles of stratification and mixing—Pilkington Bay undergoes a diel cycle of stratification and mixing, as has been observed in other tropical lakes (Talling and Lemoalle 1998). Factors that influence the depth of the surface layer can be understood from the surface energy budget. The water column is stratified to the surface or has only a thin surface layer when F_q is least; that is, when there is no cooling ($w_* = 0$) and no wind forcing (Fig. 4A,C). The surface layer deepens as F_q increases with the most rapid deepening for the largest F_q. Because F_q is based on the cube of both u_{*w} and w_*, examination of those individual terms allows assessment of the contribution of wind forcing and cooling to surface layer deepening at different times of day. Examination of the temperature record (not shown) shows that surface cooling began at 1430 h on 24 April, when w_* first exceeded 0 (Fig. 5). Consequently, surface layer deepening requires that surface heat losses exceed inputs from shortwave radiation. In Pilkington Bay, evaporation causes the greatest heat loss (Fig. 3C). Hence, wind contributes to surface layer deepening not only through direct production of turbulence but also by making the greatest contribution to heat losses at the air-water interface.

Wind also causes the thermocline to tilt, with downwelling at the downwind end of a lake. On occasion, upwelling occurred independently of wind speed and downwelling was maintained in the absence of wind speed. At these times, processes besides wind and heat loss contributed to thermocline depth. We will discuss this topic in a later section.

Strong wind forcing does not always lead to thermocline tilting. Wind speeds at ~1000 h on 26 April reached 8 m

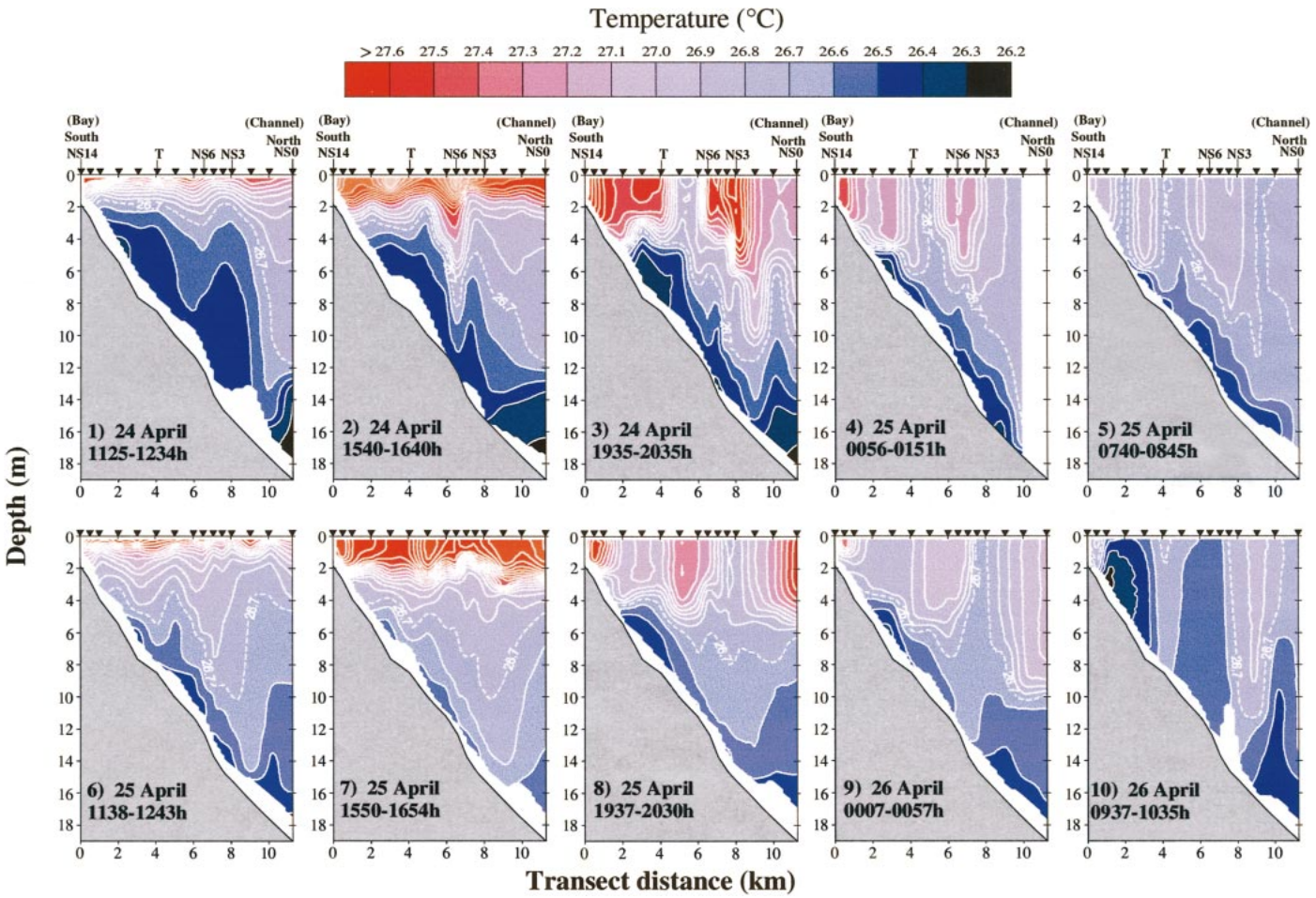

Fig. 10. Spatial variation of temperature from north to south, 24–26 April 1996, showing development of warm pools in the day, downwelling of surface waters at convergences, and persistent horizontal differences even after nocturnal cooling. Selected stations of CTD transect labeled (NS14, NS6, NS3, and NS0) and the location of the thermistor chain (T). The dashed isotherm indicates the reference temperature of 26.7°C.

s^{-1}, values similar to the other times with strong wind forcing (Fig. 2D). However, F_q equalled 75×10^{-8} m^3 s^{-3} (Fig. 4C), a value less than half that observed at the other times. Because of solar inputs, the contribution to F_q from heat loss was much less. The strong wind forcing did not cause downwelling. Instead, a shallow surface layer formed as opposed to the continuous stratification seen on calmer days (Fig. 4A).

The ratio of buoyancy flux to total kinetic energy flux was zero or close to zero in the day, which indicates that any turbulence produced was generated by wind (Fig. 4C). Once the surface layer was >1.5 m depth, the ratio was >0.5 for 92% of the time, >0.7 for 82% of the time, >0.8 for 61% of the time, and >0.9 for 32% of the time. These percentages indicate that surface layer deepening is primarily driven by heat loss. The fraction of the upper mixed layer mixed by wind is estimated by the ratio of the Monin-Obukhov length scale in water to the mixed layer depth; the ratio is equivalent to w_*^3/u_{*w}^3 (Imberger 1985). Below the depth of wind stirring, convectively driven motions dominate. Comparison of the magnitude of w_* relative to u_* (Fig. 4B) also shows that wind stirring dominates mixing in the upper mixed layer in the day. As the lake begins to cool, however, progressively more and more of the upper mixed layer is circulated by thermals induced by heat loss. For instance, between midnight and 0600 h on 25 April, w_*^3/u_{*w}^3 indicates that <50% of the upper mixed layer was circulated by wind induced motions. At times, <20% was circulated by turbulent eddies generated by wind. Only during high winds at night is the depth of mixing equivalent for motions induced by wind and by heat loss.

Rates of energy dissipation ε averaged for the mixed layer can be calculated from the surface energy budget by use of $\varepsilon = 2 \times F_q/h$ where h equals the mixed layer depth (Imberger 1985). Dissipation rates describe the intensity of turbulence in the water column. ε was between 1×10^{-6} and 5×10^{-6} m^2 s^{-3} during afternoon winds, when the energy was constrained to a shallow mixing layer, and during the strong wind forcing at night. Such values of ε are indicative of strong turbulence and are typical of values found in temperate lakes during periods of high wind forcing (MacIntyre et al. 1999). In contrast, when wind speeds were <2 m s^{-1} and mixing was dominated by heat loss, $\varepsilon = 10^{-7}$ m^2 s^{-3}, which indicates that the upper mixed layer was moderately turbulent. Similar values were found in the upper mixed layer of Lake Biwa when winds were <4 m s^{-1} or when mixing

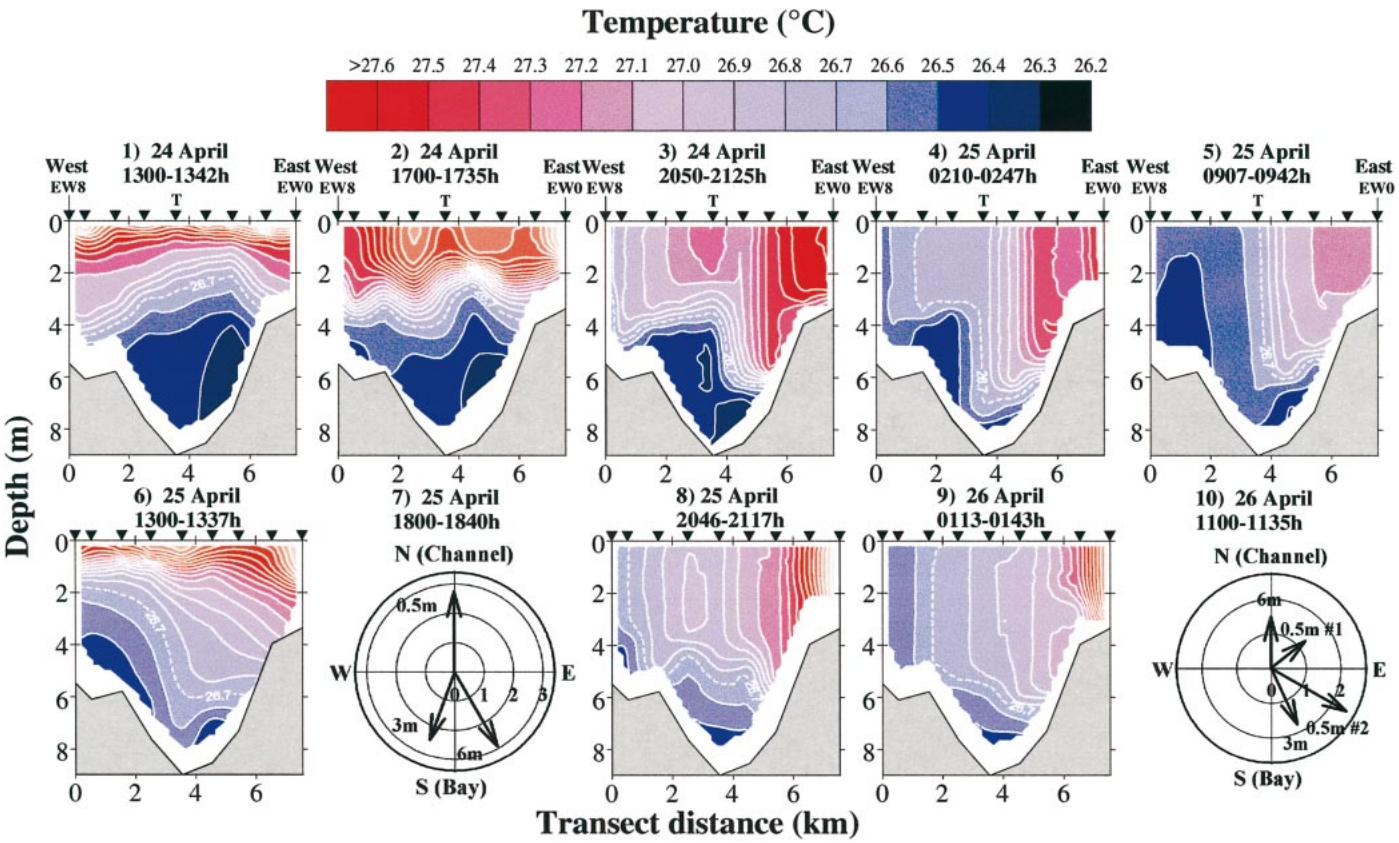

Fig. 11. Spatial variation of temperature along the east-west transect showing development of the diurnal thermocline in the afternoon, warm inflows in early evening, and spatial variations of thermocline depth due to inflows at night and subsequent gravitational readjustments in the day. Current velocities indicated by direction (° from N) and speed (cm s^{-1}) at 0.5-, 3-, and 6-m depth with measurements obtained 1800–1840 h 25 April and 1100–1135 h 26 April.

was dominated by heat loss (MacIntyre 1998; Robarts et al. 1998).

The turbulent velocity scale q for turbulence due to all processes is $(2F_q)^{1/3}$, and the timescale of mixing of the mixing layer is h/q. When temperature is stratified to the surface, mixing is minimal. For mixed layers <1.5 m, the mixing time was <2 min. Once the mixed layer depth was >1.5 m, the mixing time was always <12 min. These timescales are short when compared with the canonical values given in Denman and Gargett (1983). Timescales of mixing due to heat loss tended to be faster than those from wind, a result that, along with the Monin-Obukhov length scale comparison, indicates that mixing at night is largely caused by thermals.

Horizontal transports (differential heating and cooling and differential mixing)—Surface overflows are expected when shallow waters trap more heat than deeper ones, when water turbidity differs, and when the depth of wind mixing varies (Imberger and Parker 1985; Monismith et al. 1990). Underflows are anticipated when cooling is greater in shallow areas. We anticipated such flows in Pilkington Bay, particularly because there were north-south and east-west differences in Secchi depth and because different regions of the bay were sheltered from wind mixing depending on wind direction. In addition, Ochumba (1996) reported diel temperature differences in shallow areas of Nyanza Gulf in eastern Lake Victoria.

At times, the patterns of heating and cooling were likely to have generated the anticipated flows; at other times they did not. For instance, greater heating did occur during the day in shallow regions along both transects. Such heating should generate overflows. Greater heating was also observed in the constrictions on some days, likely because of lesser influence of wind, and overflows would be expected. However, midbay stations often had temperatures higher than surrounding waters. Shallow waters in the south and eastern bay remained warmer at night than those farther offshore; consequently, neither the frontal structures predicted by Farrow and Patterson (1993) nor the underflows predicted by Monismith et al. (1990) were likely to have occurred. Greater cooling did occur sometimes in the western bay than in midlake, but only on the morning of the last day of our study did we observe colder waters at an inshore site that could have flowed offshore.

Following the method of Sturman et al. (1999), we calculated flow speeds, U, and flushing times, τ_f, for downslope currents induced by differential cooling. $U \sim (BL_H \sin\theta/C_D)^{1/3}$ and $\tau_f = L_H^{2/3}\,(1 + \tan\theta)^{4/3}/(B \tan\theta)^{1/3}$, where B is buoyancy flux in $m^2\ s^{-3}$, L_H is horizontal distance, and θ is the bottom slope. Buoyancy fluxes from late afternoon until early morning ranged from 10^{-8} to $10^{-7}\ m^2\ s^{-3}$, bottom slope averaged

11°, and the horizontal distance was 4 km for the velocity calculation and 2 km for the flushing time calculation. Calculated velocities ranged from 0.06 to 0.14 m s^{-1} and travel times ranged from 10 to 24 h, but flushing times of the inshore embayments would have been on the order of 2.5–5 d. Cool water arrived at the thermistor station at 1930 h 24 April and at 2230 h 25 April. Given that formation of cool waters inshore was infrequent, that the flushing times indicate only a small volume of water would reach midlake stations, and that movement of the cool deep water was coupled with thermocline deflections, as discussed below, we believe that the formation of gravity currents by differential cooling was not an important mechanism for exchange in Pilkington Bay at this time. However, because of the wide variations in surface temperatures, surface overflows would have been frequent with return flows at other depths.

Upwellings and downwellings occurred in Pilkington Bay because of convergence and divergence of water masses. Farrow and Patterson's (1993) model indicates that upwelling and downwelling fronts will occur when near-shore regions shift from more rapid heating to more rapid cooling than offshore waters. As discussed above, however, the near-shore regions tended to remain warmer than those offshore. Consequently, other mechanisms may have been operative. For instance, the downwelling on the afternoon of 24 April (Fig. 10, transect 2) occurred after the onset of winds and was likely caused by a convergence of the slightly cooler waters in the bay and the warmer waters in the constriction. In Pilkington Bay, warm water penetrated a depth of 2 m within 3 h, which suggests downwelling velocities on the order of mm s^{-1}, similar to those modeled in another polymictic water body (Rueda et al. in press; Rueda and Schladow pers. comm.). To balance the downwelling, upwelling occurred to the south. This mechanism will cause exchanges between surface and deeper waters on subdaily timescales.

The temperature difference between the warm waters in the constriction and the bay likely generated an inflow into the bay at night. The warmest temperatures on the east-west transect in late afternoon occurred in the east (Fig. 11). Although some of the warm water likely originated near shore because of greater turbidity in the eastern bay, by 2050 h the pool of warm water extended 2–3 km into the bay, had a depth of 6 m, and had persisted for several hours. Temperatures in the upper 6 m exceeded 27.3°C between Buvuma Channel and Pilkington Bay in early evening on 24 April (Fig. 10, transect 3). Similar warm temperatures would also have been likely in the other constriction and are a likely source of the warm water.

Several mechanisms may have caused the inflow. Wind speeds prior to 2050 h ranged from 4 to 6 m s^{-1}, with gusts to nearly 8 m s^{-1}. Surface drift currents are ~3% of wind speed; hence, average surface current speeds would have been ~ 0.2 m s^{-1}. Consequently, the inflow could have been generated by wind. At steady state, current speeds induced by horizontal temperature differences can be estimated as $u \sim (g\alpha\ \Delta T\ H_I)^{1/2}$, where α is the thermal coefficient of expansion (at 27°C, $\alpha = 2.8 \times 10^{-4}$ °C^{-1}), ΔT is the horizontal temperature difference, and H_I is the thickness of the intrusion (Monismith et al. 1990; Nepf and Oldham 1997). On the basis of ΔT = 0.6°C and a layer thickness of 5 m at 2050 h (Fig. 11, transect 3), the velocity would have been 0.1 m s^{-1}. Given a distance of 2.5–3 km between the eastern constriction and EW2, the travel time for the warm water would have been 4–6 h. Consequently, the inflow could have been generated by the horizontal pressure gradient. Any buildup of water in Hannington Bay itself caused by wind-induced currents or large-scale wave motions elsewhere in the lake could also have generated a flow into Pilkington Bay.

The inflow of water from the constriction appears to have caused or contributed to thermocline downwelling. On east-west transect 3 (Fig. 11), the thermocline sloped upward from west to east until midbasin, where it downwelled 2 m in ~500 m. Although wind mixing could have been greater in the eastern half of the basin and the 8 m s^{-1} wind at 2300 h may have contributed to downwelling, that strong wind only persisted for 1 h, and the thermocline remained downwelled in the east for several hours after wind speeds dropped to <5 m s^{-1}. Greater wind mixing in the east would also have led to a more rapid rate of cooling, but waters are warmer to the east. Hence, it is likely that neither wind nor cooling alone contributed to the persistent downwelling.

We hypothesize that the inflows of warm water into the eastern bay generated a pressure force P that contributed to and maintained thermocline tilting. We calculated the pressure force due to a horizontal temperature gradient as $P = \rho g\alpha\ (dT/dx)\ H_I^2$ (Nepf and Oldham 1997). At 2050–2125 h on 24 April, the temperature difference between the station where the strongest thermocline tilting occurred and the shore was 0.6°C, the distance to shore was 3 km, and the layer thickness was 5 m. At 0210–0247 h on April 25, the temperature gradient between the thermistor station and EW2 was ~0.6°C, the distance was ~2 km, and the well-mixed layer was ~5 m deep. Consequently, the pressure at the first time was 0.014 N m^{-2}, and that at the second was 0.02 N m^{-2}. The first was equivalent to a wind speed of 3.2 m s^{-1} and the second to one of 4 m s^{-1}. Consequently, pressure from the wind and the inflow likely acted together to cause the thermocline depression in the east.

The westward movement of cool deep water (<26.5°C) was also a likely response to the horizontal pressure gradient. This cool water moved farther west as the inflow penetrated (Fig. 11, transects 2–5). The onset of heating the next day reduced the spatial differences in temperature along the east-west transect and relaxed the horizontal pressure gradient. Consequently, the cool water flowed eastward. The drogue measurements (Fig. 11, transect 7) support this interpretation.

Lateral advection of these deep water masses apparently caused thermocline up- or downwelling and generated high-frequency waves. For instance, thermocline upwelling occurred at 1830 h on 24 April (Fig. 5) and at 1800 h on 25 April (Fig. 7), with only a slight reduction in wind speeds. In both cases, cooler water had moved to the thermistor chain station (Figs. 5, 10, transects 3 and 8; Fig. 11, transects 6–8). The relaxation of the upwelling at 2000 h (Fig. 7) due to lateral transport of the cool water away from the thermistor station led to formation of a train of high-frequency waves.

Water also flowed from Buvuma Channel into the bay.

The upward movement of the 26.8°C isotherm between transects 6 and 7 (Fig. 10) and the subsequent upward movement of the 26.7°C isotherm between transects 7 and 8 (Fig. 10) suggests that waters with temperatures between 26.6°C and 26.8°C flowed into the constriction at depths between 4 and 8 m (Fig. 10, transects 6–8). Because the upward movements of these isotherms occurred in the constriction but not in either the bay or the channel indicates an inflow rather than heating. The time series data at the thermistor station (Fig. 7) provides evidence that water entered the bay. Isotherm displacements at 4–6 m depth (26.7°C and 26.8°C), as well as the isotherms a degree above and below these, were out of phase from 1430 to 1630 h (Fig. 7). We interpret these motions as indicative of inflows of water of intermediate temperature. The drogue measurements are supportive of this interpretation as flows were to the southeast at 3 m and to the southwest at 6 m depth at this time. We do not know the mechanism that led to this exchange.

Internal waves, vertical transports, and intrusions—Waves with periods of 5–45 min were generated in the thermocline as wind forcing decreased (Fig. 6) and as the thermocline rapidly downwelled (Fig. 7). Five of the temperature loggers (3.5, 4, 4.5, 5, and 5.5 m) recorded the wave train after the downwelling. These latter waves are broader at their troughs than at their crests, a feature often found in nonlinear waves (Hunkins and Fliegel 1973). Recently, Stevens (1999) observed high-frequency waves such as these in a small reservoir. He provided evidence that they increase shear in the thermocline and therefore may increase the potential for vertical mixing in the thermocline. Hebert et al. (1992) and Moum et al. (1992) found a high correlation between the incidence of turbulence and high-frequency internal waves. The high-frequency waves in Pilkington Bay may provide a mechanism for vertical transport across the thermocline; the likelihood of this transport is even greater if the waves are nonlinear (Innal et al. 2000).

Breaking of internal waves at the sediment boundary, or any process that causes localized mixing in a stratified fluid, can lead to intrusions of well-mixed water into the main body of a lake (Browand et al. 1987; Thorpe 1998). Mixing at boundaries can occur if waves with frequencies critical for breaking impinge on the boundary (Ivey and Nokes 1989). Critical frequencies f_c for wave breaking are equal to the buoyancy frequency N at a depth times bottom slope θ ($f_c = N\theta$; DeSilva et al. 1997). We calculated critical frequencies using profiles of N taken over a diurnal cycle and bottom slopes calculated from our bathymetry. Bottom slopes in the bay are typically low but reach 0.02 m m^{-1} in a few locations; slopes reach 0.1 m m^{-1} in the constriction. Within the bay itself, wave breaking was likely in $<$5% of the basin; however, wave breaking was likely to occur between 1 and 6 m depth within the constrictions (not shown). Consequently, intrusions of water from the constrictions into the bay are possible. In contrast to lakes with a larger area of steeply sloping bottom, this mechanism is less likely to be of importance in Pilkington Bay for coupled vertical-horizontal transport.

Conclusions

This data set from Pilkington Bay provides the first surface energy budget for a tropical lake over diurnal time scales and is one of the most complete data sets showing spatial variation of thermal structure over a short time period. Because of the intensive sampling in this geometrically complex embayment, the data set allows assessment of the important physical processes, the flows generated, and their implications for transport of solutes and particles.

Pilkington Bay is a dynamic system. Stratification develops in the morning and is highly stable by early afternoon ($N \sim 40$ cph). Such strong stratification is similar to that observed across the seasonal thermocline in temperate and arctic lakes. Despite high solar irradiances, heat losses occur from midafternoon until midmorning the following day, and stratification is eroded on a daily basis. Except for a ~6-h period around solar noon, cooling begins as soon as the wind increases. Because of the warm surface waters, the cooling is largely due to evaporation. Consequently, not only u_{*w} but also w_* tend to increase with wind forcing. This behavior differs from that observed in lakes with colder surface waters where wind forcing and heat loss are not as tightly coupled (MacIntyre and Kling unpubl. data). This greater and more persistent contribution of heat loss to mixed layer deepening in tropical lakes may be a contributing factor to the greater mixed layer depth for tropical versus temperate lakes of the same fetch (Kling 1988).

Spatial differences in the rates of heating and cooling and in the depth of wind mixing cause fronts to develop on spatial scales of kilometers. Wind-induced motion of these fronts leads to vertical exchanges on subdaily timescales as surface waters downwell and deeper waters upwell. In addition, movement of these fronts in the upper water column induces thermocline downwelling and lateral movement of deep waters. Movement of the deep waters causes additional thermocline up- and downwellings, some of which spawn high-frequency waves that may have sufficient shear to cause vertical mixing and some of which are likely to break in the constrictions and cause additional vertical fluxes and lateral advection. The flows thus generated are more complex and influence a larger area than anticipated from models of differential heating, cooling, and wind mixing.

Accurate assessment of mixed layer depth is required for models of mixed layer dynamics (Brainerd and Gregg 1993*b*), internal wave dynamics in the thermocline (Hodges et al. 2000), and phytoplankton photosynthesis (Geider et al. 1998). These results from Pilkington Bay indicate that mixed layer and thermocline depth depend not only on surface energy budgets at the site of measurement but also on processes generated by different rates of heating and cooling and different wind stresses elsewhere in a basin. Mixed layer depth at night is not only set by convection but also by the movement of intrusions, and restratification in the day does not only depend on heating but also on gravitational adjustment of horizontal density differences. Descriptions of thermocline motions require not only consideration of pressure forces from wind but also those from persistent horizontal pressure gradients such as are created by inflows with different temperatures.

Accurate estimates of surface energy budgets are important for regional models of water balance and estimates of gas flux. Both require accurate estimation of evaporation. Surface temperature variations in temperate lakes can cause errors in evaporation estimates on the order of 10% (LeDrew and Reid 1982). In tropical water bodies, where evaporation rates can be even higher than in temperate water bodies, and large differences in surface temperatures occur, errors in estimates may be even higher. The gas transfer velocity depends on the turbulence near the air-water interface and is often based on wind speed alone (MacIntyre et al. 1995). Our results from Pilkington Bay indicate that the turbulent velocity scale due to heat loss exceeds that due to wind stress for long periods of the day. Consequently, estimates of the gas transfer coefficient are likely to be too low by a factor of two for tropical water bodies (MacIntyre et al. 2001).

Multiple fronts due to large temperature differences in Pilkington Bay create a diversity of habitats for phytoplankton as well as sites with different rates of biological and chemical activity. Upwellings and downwellings induced by convergences of fronts occur frequently during the day and penetrate the diurnal thermocline. They are likely to be a more important mechanism for vertical exchange than turbulent mixing in the day and provide a mechanism whereby phytoplankton in surface waters are moved away from damaging irradiances and whereby phytoplankton, bacteria, and solutes from middepths in the water column reach the surface. At night, vertical exchange is induced by convection caused by heat loss, but spatial heterogeneity is maintained because of the spatially variable rates of heating in the day.

Lateral motions of cool, anoxic bottom waters can lead to spatial heterogeneity in rates of microbial activity or nutrient release from sediments. In Pilkington Bay, as in other water bodies with localized anoxia, results of studies of denitrification, phosphorus supply, or changes in cell nutrient status will be dependent on sampling location. Determining the ecological consequences of the changing physical structure in the water column due to spatial and temporal variations in rates of heating, cooling, and wind stress at the water surface is a challenge ahead for understanding controls on ecosystem productivity.

References

AMOROCHO, J., AND J. J. DEVRIES. 1980. A new evaluation of the wind stress coefficient over water surfaces. J. Geophys. Res. **85:** 433–442.

ANIS, A., AND J. N. MOUM. 1994. Prescriptions for heat flux and entrainment rates in the upper ocean during convection. J. Phys. Oceanogr. **24:** 2142–2155.

———, AND ———. 1995. Surface wave-turbulence interactions—scaling epsilon(z) near the sea surface. J. Phys. Oceanogr. **25:** 2025–2045.

ANDERSON, E. R. 1954. Energy budget studies, water loss investigations—Lake Hefner studies. U. S. Geol. Surv. Prof. Paper **269:** 71.

BOOTSMA, H. A., AND R. E. HECKY. 1993. Conservation of the African Great Lakes—a limnological perspective. Conserv. Biol. **7:** 644–656.

BRAINERD, K. E., AND M. C. GREGG. 1993*a*. Diurnal restratification and turbulence in the oceanic surface mixed layer. 1. Observations. J. Geophys. Res. **98:** 22645–22656.

———, AND ———. 1993*b*. Diurnal restratification and turbulence in the oceanic surface mixed layer. 2. Modeling. J. Geophys. Res. **98:** 22657–22664.

BROWAND, F. K., D. GUYOMAR, AND S.-C. YOON. 1987. The behavior of a turbulent front in a stratified fluid: Experiments with an oscillating grid. J. Geophys. Res. **92:** 5329–5341.

BRUTSAERT, W. H. 1982. Evaporation into the atmosphere: Theory, history, and applications. D. Reidel.

CHEN, C. T., AND F. J. MILLERO. 1977. The use and misuse of pure water PVT properties for lake waters. Nature **266:** 707–708.

COATES, M. J., AND J. FERRIS. 1994. The radiatively driven natural convection beneath a floating plant layer. Limnol. Oceanogr. **39:** 1186–1194.

CRILL, P. M., AND OTHERS. 1988. Tropospheric methane from an Amazonian floodplain lake. J. Geophys. Res. **93:** 1564–1570.

DEARDOFF, J. W. 1970. Convective velocity and temperature scales for unstable planetary boundary layer and for Rayleigh convection. J. Atmos. Sci. **27:** 1211–1213.

DENMAN, K. L., AND A. E. GARGETT. 1983. Time and space scales of vertical mixing and advection of phytoplankton in the upper ocean. Limnol. Oceanogr. **28:** 801–815.

DESILVA, I. P. D., J. IMBERGER, AND G. N. IVEY. 1997. Localized mixing due to a breaking internal wave ray at a sloping bed. J. Fluid Mech. **350:** 1–27.

FARROW, D. E., AND J. C. PATTERSON. 1993. On the response of a reservoir sidearm to diurnal heating and cooling. J. Fluid Mech. **246:** 143–161.

GEIDER, R. J., H. L. MACINTYRE, AND T. M. KANA. 1998. A dynamic regulatory model of phytoplankton acclimation to light, nutrients, and temperature. Limnol. Oceanogr. **43:** 679–694.

GOUDSMIT, G., F. PEETERS, M. GLOOR, AND A. WUEST. 1997. Boundary versus internal diapycnal mixing in stratified, natural waters. J. Geophys. Res. **102:** 27903–27914.

HARE, L., AND J. C. H. CARTER. 1984. Diel and seasonal physicochemical fluctuations in a small natural West African lake. Freshw. Biol. **14:** 597–610.

HEBERT, D., J. N. MOUM, C. A. PAULSON, AND D. R. CALDWELL. 1992. Turbulence and internal waves at the equator. Part II. Details of a single event. J. Phys. Oceanogr. **22:** 1346–1356.

———, F. W. B. BUGENYI, P. OCHUMBA, J. F. TALLING, R. MUGIDDE, M. GOPHEN, AND L. KAUFMAN. 1994. Deoxygenation of the deep water of Lake Victoria, East Africa. Limnol. Oceanogr. **39:** 1476–1481.

HECKY, R. E. 1993. The eutrophication of Lake Victoria. Verh. Internat. Verein. Limnol. **25:** 39–48.

HENDERSON-SELLERS, B. 1986. Calculating the surface energy balance for lake and reservoir modeling: A review. Rev. Geophys. **24:** 625–649.

HICKS, B. B. 1972. Some evaluations of drag and bulk transfer coefficients over water bodies of different sizes. Boundary-Layer Meteorol. **3:** 201–213.

———. 1975. A procedure for the formulation of bulk transfer coefficients over water. Boundary-Layer Meteorol. **8:** 515–524.

HODGES, B. R., J. IMBERGER, A. SAGGIO, AND K. B. WINTERS. 2000. Modeling basin scale internal waves in a stratified lake. Limnol. Oceanogr. **45:** 1603–1620.

HUNKINS, K., AND M. FLIEGEL. 1973. Internal undular surges in Seneca Lake: A natural occurrence of solitons. J. Geophys. Res. **78:** 539–548.

IMBERGER, J. 1985. The diurnal mixed layer. Limnol. Oceanogr. **30:** 737–770.

———, AND G. PARKER. 1985. Mixed layer dynamics in a lake exposed to a spatially variable wind field. Limnol. Oceanogr. **39:** 473–488.

———, AND J. C. PATTERSON. 1990. Physical limnology. Adv. Appl. Mech. **27:** 303–475.

INALL, M. E., T. P. RIPPETH, AND T. J. SHERWIN. 2000. Impact of nonlinear waves on the dissipation of internal tidal energy at a shelf break. J. Geophys. Res. **105:** 8687–8705.

ISHIKAWA, T., AND M. TANAKA. 1993. Diurnal stratification and its effects on wind-induced currents and water qualities in Lake Kasumigaura, Japan. J. Hydraulic Res. **31:** 307–322.

IVEY, G. N., AND R. I. NOKES. 1989. Vertical mixing due to the breaking of critical internal waves on sloping boundaries. J. Fluid Mech. **204:** 479–500.

JAMES, W. F., AND J. W. BARKO. 1991. Littoral-pelagic phosphorus dynamics during nighttime convective circulation. Limnol. Oceanogr. **36:** 949–960.

JELLISON, R. S., AND J. M. MELACK. 1993. Meromixis in hypersaline Mono Lake, California. 1: Vertical mixing and density stratification during the onset, persistence, and breakdown of meromixis. Limnol. Oceanogr. **38:** 1008–1019.

KAUFMAN, L. S. 1992. Catastrophic change in species-rich freshwater ecosystems, the lessons of Lake Victoria. BioScience **42:** 846–852.

———. 1993. The challenge of the world's great lakes. Conserv. Biol. **7:** 447–449.

KIM, J. W. 1976. A generalized bulk model of the oceanic mixed layer. J. Phys. Oceanogr. **6:** 686–695.

KLING, G. W. 1988. Comparative transparency, depth of mixing, and stability of stratification in lakes of Cameroon, West Africa. Limnol. Oceanogr. **33:** 27–40.

KLING, G. W., W. C. EVANS, M. L. TUTTLE, AND G. TANYILEKE. 1989. The evolution of thermal structure and water chemistry in Lake Nyos. J. Volcanol. Geotherm. Res. **39:** 151–166.

LEDREW, E. F., AND P. D. REID. 1982. The significance of surface temperature patterns on the energy balance of a small lake in the Canadian Shield. Atmosphere-Ocean **20:** 101–115.

MACINTYRE, S. 1993. Vertical mixing in a shallow, eutrophic lake—possible consequences for the light climate of phytoplankton. Limnol. Oceanogr. **38:** 798–817.

———. 1996. Turbulent eddies and their implications for phytoplankton within the euphotic zone of Lake Biwa. Jpn. J. Limnol. **57:** 395–410.

———. 1998. Turbulent mixing and resource supply to phytoplankton, p. 539–567. *In* J. Imberger [ed.], Physical processes in lakes and oceans. Coastal and estuarine studies 54. American Geophysical Union.

———, W. EUGSTER, AND G. W. KLING. 2001. The critical importance of buoyancy flux for gas flux across the air-water interface, p. 135–139. *In* M. A. Donelan, W. M. Drennan, E. S. Saltzman, and R. Wanninkhof [eds.], Gas transfer at water surfaces. Geophysical monograph 127. American Geophysical Union.

———, K. M. FLYNN, R. JELLISON, AND J. R. ROMERO. 1999. Boundary mixing and nutrient fluxes in Mono Lake, California. Limnol. Oceanogr. **44:** 512–529.

———, AND R. JELLISON. In press. Nutrient fluxes from upwelling and enhanced turbulence at the top of the pycnocline in Mono Lake, California. Hydrobiolgia.

———, AND J. M. MELACK. 1982. Meromixis in an equatorial African soda lake. Limnol. Oceanogr. **27:** 595–609.

———, AND ———. 1984. Vertical mixing in Amazon floodplain lakes. Verh. Int. Ver. Limnol. **22:** 1283–1287.

———, AND ———. 1988. Frequency and depth of vertical mixing in an Amazon floodplain lake (L. Calado, Brazil). Verh. Int. Ver. Limnol. **23:** 80–85.

———, AND ———. 1995. Vertical and horizontal transport in lakes—linking littoral, benthic, and pelagic habitats. J. North Am. Benthol. Soc. **14:** 599–615.

———, R. WANNINKHOF, AND J. CHANTON. 1995. Trace gas exchange across the air-water interface in freshwater and coastal marine environments, p. 52–97. *In* P. Matson and R. Harriss [eds.], Biogenic trace gases: Measuring emissions from soil and water. Blackwell.

MELACK, J. M. 1982. Photosynthetic activity and respiration in an equatorial African soda lake. Freshw. Biol. **12:** 381–400.

MILLERO, F. J., AND A. POISSON. 1981. International one-atmosphere equation of state of seawater. Deep-Sea Res. **28:** 625–629.

MONIN, A. S., AND A. M. OBUKHOV. 1954. Basic laws of turbulent mixing in the atmosphere near the ground. J. Akad. Nauk. SSR Geofiz. Inst. **24:**163–187.

MONISMITH, S. G. 1985. Wind-forced motions in stratified lakes and their effect on mixed-layer shear. Limnol. Oceanogr. **30:** 771–783.

———. 1986. An experimental study of the upwelling response of stratified reservoirs to surface shear stress. J. Fluid Mech. **171:** 407–439.

———. 1987. The modal response of reservoirs to wind stress. J. Hydrol. Div. ASCE **113:** 1290–1326.

———, J. IMBERGER, AND M. L. MORISON. 1990. Convective motions in the sidearm of a small reservoir. Limnol. Oceanogr. **35:** 1676–1702.

MOUM, J. N., D. HEBERT, C. A. PAULSON, AND D. R. CALDWELL. 1992. Turbulence and internal waves at the Equator. Part I: Statistics from towed thermistors and a microstructure profiler. J. Phys. Oceanogr. **22:** 1330–1345.

NEPF, H. M., AND C. E. OLDHAM. 1997. Exchange dynamics of a shallow contaminated wetland. Aquat. Sci. **59:** 193–213.

OCHUMBA, P. B. 1996. Measurement of water currents, temperature, dissolved oxygen and winds in the Kenyan Lake Victoria, p. 155–167. *In* T. C. Johnson and E. O. Odada [eds.], The limnology, climatology and paleoclimatology of the East African Great Lakes. Gordon and Breach.

PARKER, G. J., AND J. IMBERGER. 1986. Differential mixed-layer deepening in lakes and reservoirs, p. 63–92. *In* P. De Deckker and W. D. Williams [eds.], Limnology in Australia. Dr. W. Junk.

PAULSON, C. A. 1970. The mathematical representation of wind speed and temperature profiles in the unstable atmospheric surface layer. J. Appl. Meteorol. **9:** 857–861.

POND, S., D. B. FISSEL, AND C. A. PAULSON. 1974. A note on bulk aerodynamic coefficients for sensible heat and moisture fluxes. Boundary-Layer Meteorol. **6:** 333–339.

POWELL, T. M., M. H. KIRKISH, P. J. NEALE, AND P. J. RICHERSON. 1984. The diurnal cycle of stratification in Lake Titicaca: Eddy diffusion. Verh. Int. Ver. Limnol. **22:** 1237–1243.

RAYNER, K. N. 1981. Diurnal energetics of a diurnal surface layer. University of Western Australia Centre for Water Research Reference ED-80-005.

ROBARTS, R. D., M. J. WAISER, O. HADAS, T. ZOHARY, AND S. MACINTYRE. 1998. Relaxation of phosphorus limitation due to typhoon-induced mixing in two morphologically distinct basins of Lake Biwa, Japan. Limnol. Oceanogr. **43:** 1023–1036.

RUEDA, F. J., S. G. SCHLADOW, S. G. MONISMITH, AND M. T. STACEY. In press. The internal dynamics of a large polymictic lake. Part I. Field observations. J. Hydraulic Engineering.

SAGGIO, A., AND J. IMBERGER. 1998. Internal wave weather in a stratified lake. Limnol. Oceanogr. **43:** 1780–1795.

SIPPEL, S. J., S. K. HAMILTON, AND J. M. MELACK. 1992. Inundation area and morphometry of lakes on the Amazon River floodplain, Brazil. Archiv Hydrobiol. **123:** 385–400.

STEVENS, C. 1999. Internal waves in a small reservoir. J. Geophys. Res. **104:** 15777–15788.

STURMAN, J. J., G. N. IVEY, AND J. R. TAYLOR. 1996. Convection in a long box driven by heating and cooling on the horizontal boundaries. J. Fluid Mech. **30:** 61–87.

TALLING, J. F., AND J. LEMOALLE. 1998. Ecological dynamics of tropical inland waters. Cambridge Univ. Press.

THORPE, S. A. 1998. Some dynamical effects of sloping sides of lakes, p. 441–460. *In* J. Imberger [ed.], Physical processes in lakes and oceans. Coastal and Estuarine Studies 54. American Geophysical Union.

Received: 4 July 2000
Accepted: 31 October 2001
Amended: 2 January 2002